Electronic Supplementary Material (ESI) for Journal of Materials Chemistry B.

Supplementary Information

Facile synthesis of superparamagnetic nickel-doped iron oxide nanoparticles as high-performance T_1 contrast agents for magnetic resonance imaging

Chichong Lu,[1 *] *Xue Xu*,[1] *Tingting Zhang*,[1] *Zhijie Wang*,[1,2] *Yuyun Chai*[1]

[1] Department of Chemistry, College of Chemistry and Materials Engineering, Beijing Technology and Business University, Beijing 100048, P. R. China.

[2] CAS Key Laboratory for Biomedical Effects of Nanomaterial and Nanosafety, Institute of High Energy Physics, Chinese Academy of Science (CAS), Beijing 100049, P. R. China.

* Email: luchichong@btbu.edu.cn

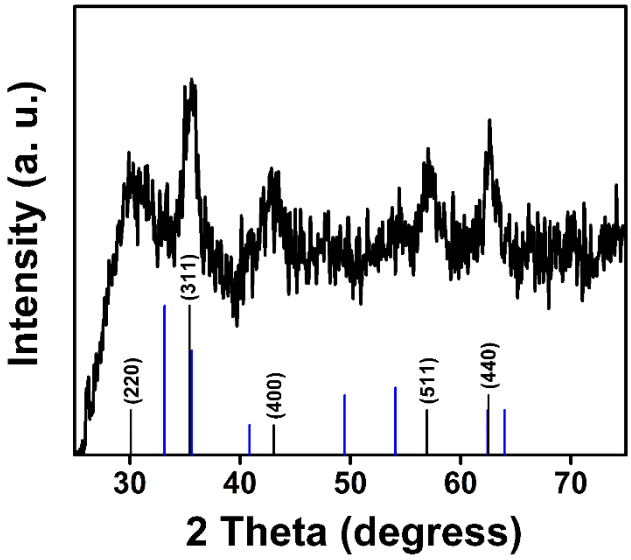

Figure S1. XRD pattern of NiIO NPs. Bars: JCPDS card data for Fe_3O_4 (No.19-0629, black) and Fe_2O_3 (No. 33-0664, blue).

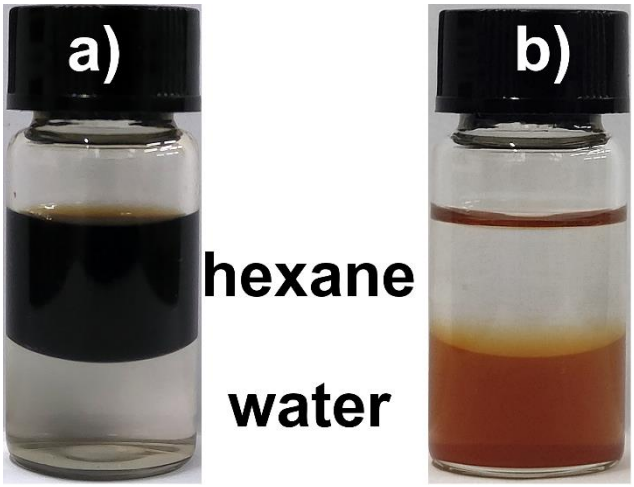

Figure S2. Photographs of (a) oleic-acid-capped NiIO NPs soluiton and (b) PEG-phospahste-modified NiIO NPs soluiton.

Figure S3. Photographs of NiIO NPs powder.

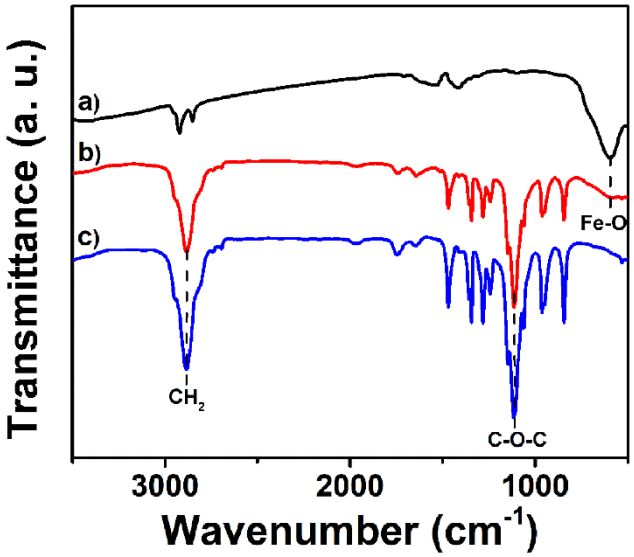

Figure S4. FT-IR spectra of (a) as-synthesized $Ni_{0.31}Fe_{2.69}O_4$ NPs, (b) PEG@ $Ni_{0.31}Fe_{2.69}O_4$ NPs and (c) carboxyl–PEG–phosphoric acid ligand. The absorption peaks at 2920 cm^{-1} and 2870 cm^{-1} are caused by the stretching and bending vibration of C–H. The absorption peaks at 1552 cm^{-1} and 1428 cm^{-1} are speculated as asymmetric and symmetric stretching vibrations of carboxylate to the surface iron of NPs. All NPs have strong bands at about 580 cm^{-1}, which is related to the stretching vibration of Fe–O in iron oxide. Compared to as-synthesized NPs, PEG@NiIO NPs exhibit the characteristic stretching vibrations of methylene (–CH_2–) around 2887 cm^{-1} and C–O–C bond around 1110 cm^{-1}, indicating successful PEG coating.

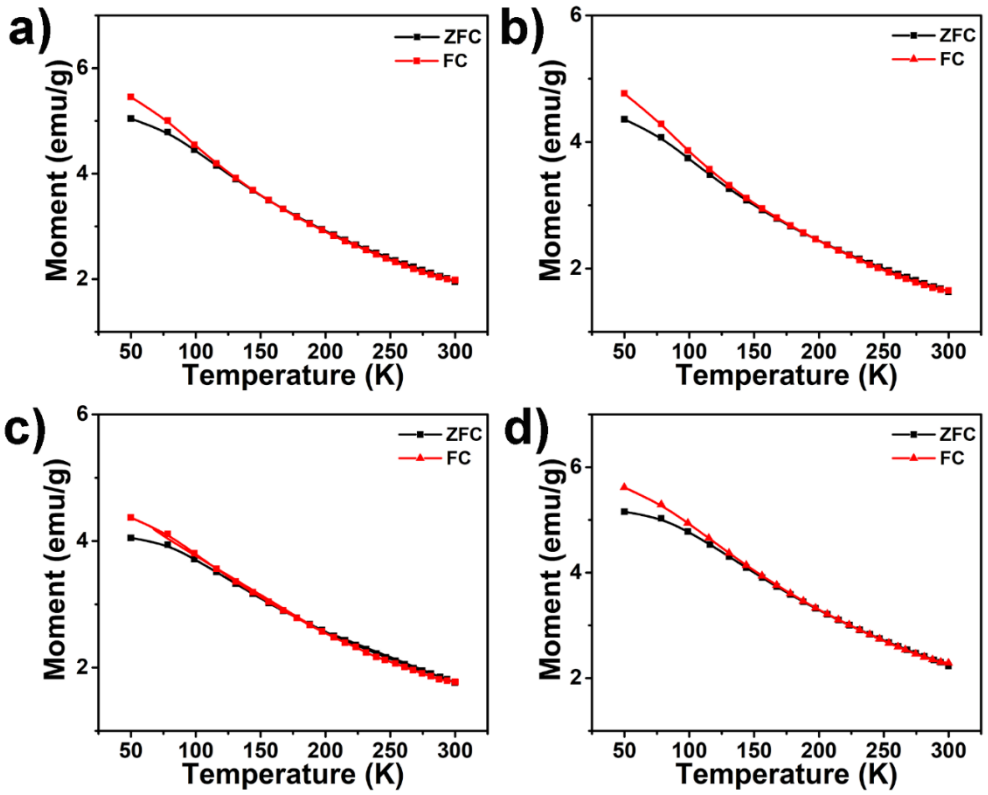

Figure S5. FC/ZFC curves of (a) $Ni_{0.12}Fe_{2.88}O_4$ NPs, (b) $Ni_{0.27}Fe_{2.73}O_4$ NPs, (c) $Ni_{0.31}Fe_{2.69}O_4$ NPs and (d) $Ni_{0.40}Fe_{2.60}O_4$ NPs.

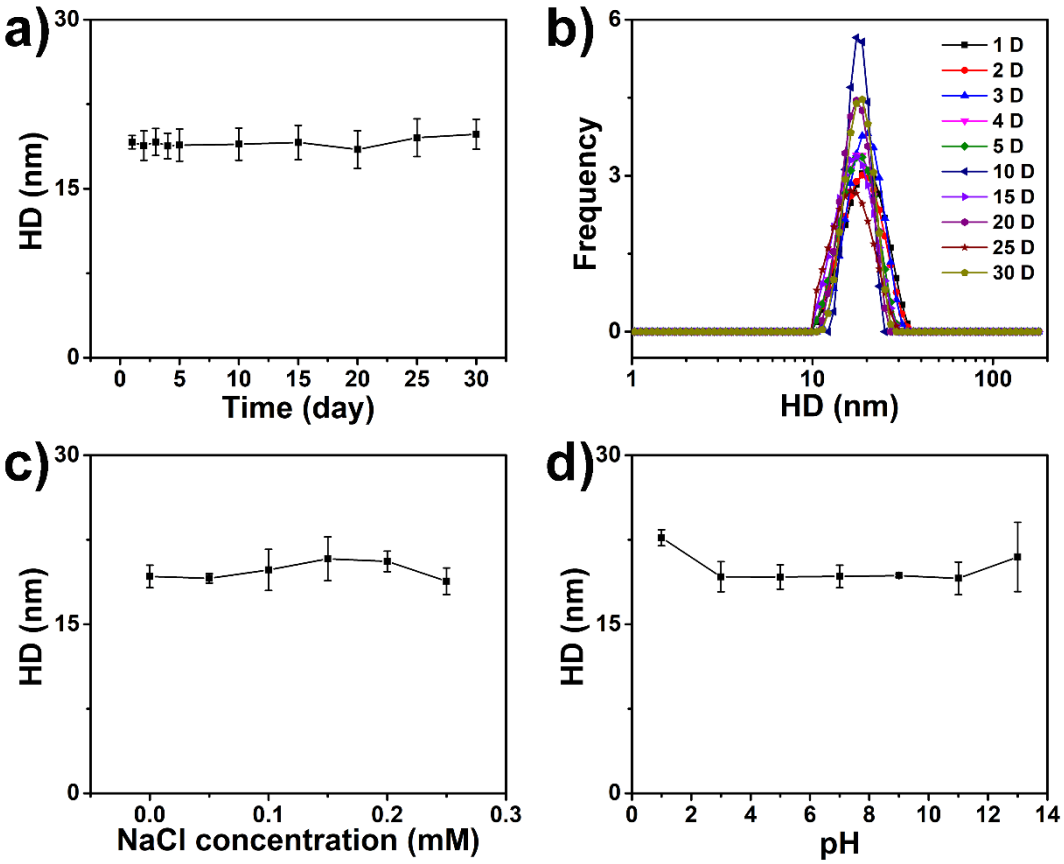

Figure S6. (a) Hydrodynamic diameter and (b) size distribution of NiIO NPs in aqueous solution at room temperature over long-term. Hydrodynamic diameter of NiIO NPs (c) in NaCl solutions of different concentrations and (d) in solution of different pH at room temperature.

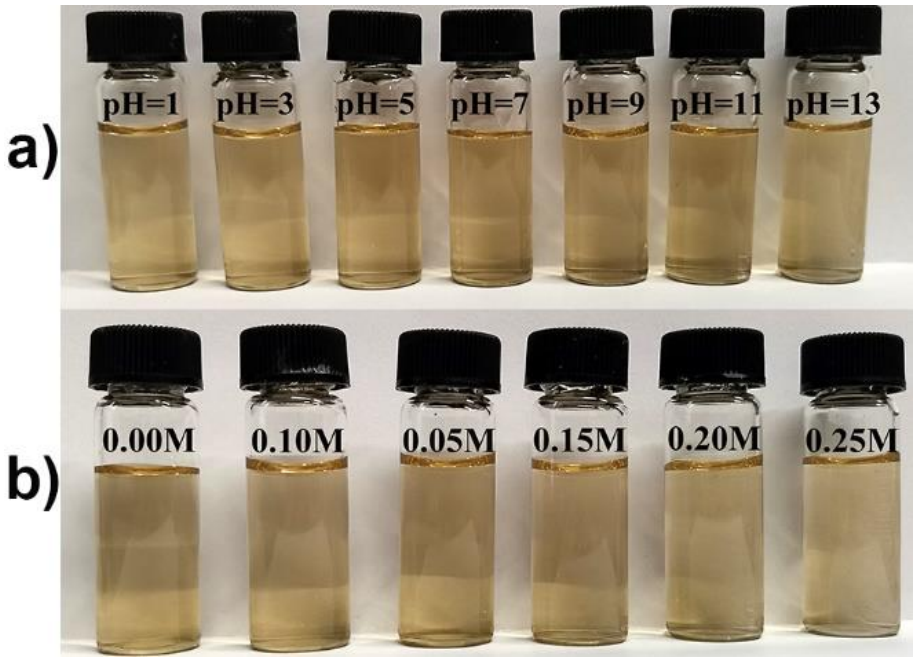

Figure S7. Photographs of modified $Ni_{0.31}Fe_{2.69}O_4$ NPs dispersed in (a) solutions of different pH and (b) NaCl solutions of different concentrations at room temperature.

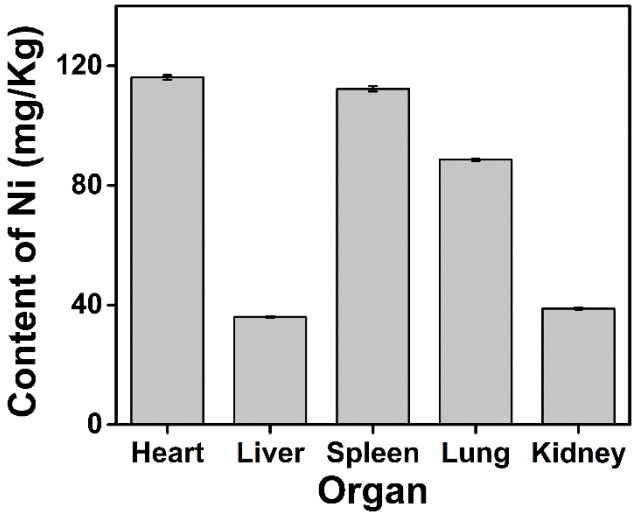

Figure S8. Content of nickel in heart, liver, spleen, lung and kidney, respectively. The tissue was digested (digestion process :120℃ for 5 minutes, 150℃ for 5 minutes, 190℃ for 10 minutes), and the content of nickel in the solution was determined by ICP-AES. The nickel content was 116.16, 36.04, 112.34, 88.61 and 38.82 mg [Ni] kg^{-1} in heart, liver, spleen, lung and kidney tissues, respectively. The high concentration in the heart tissue indicates that NiIO NPs was still circulating in the blood, suggesting their potential for MR angiography. The concentration was high in the spleen tissue, which was consistent with MRI results. The mean concentration of nickel in liver tissue is not high because the liver is the largest and therefore has the highest total mass of nickel.

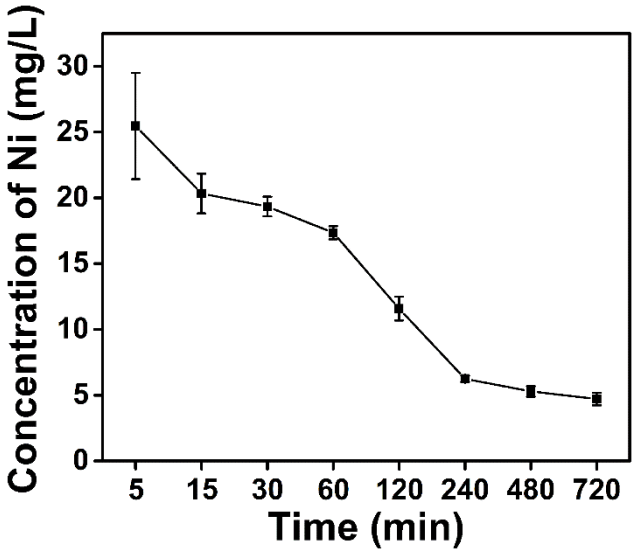

Figure S9. Concentration of nickel in blood of mice at different times.

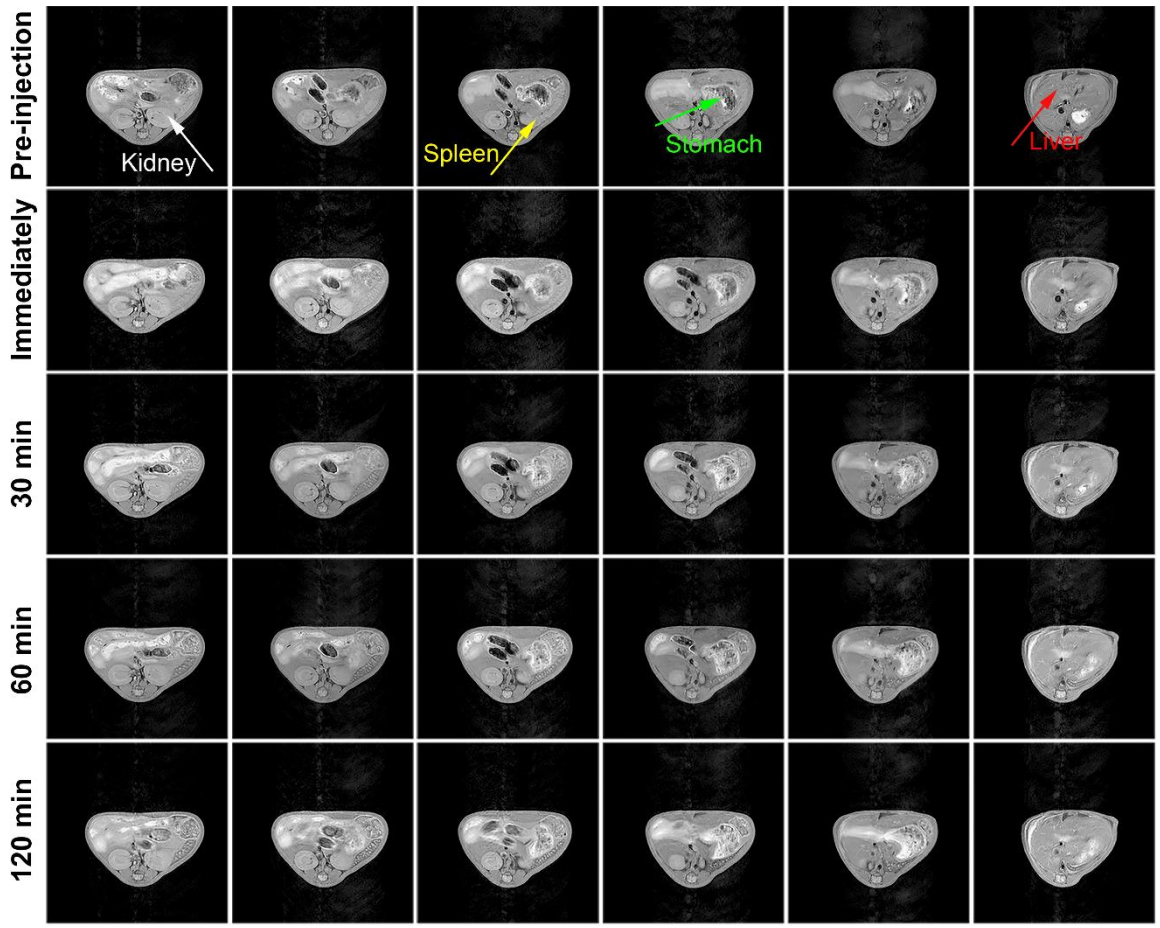

Figure S10. The transverse planes of T_1- weighted MR images of mice pre-injection, immediately after injection and 30, 60 and 120 min after injection of $Ni_{0.31}Fe_{2.69}O_4$ NPs via the tail vein (1.5 mg [Fe + Ni] kg^{-1} mouse body weight). The white, yellow, green and red arrow correspond to kidney, spleen, stomach and liver, respectively.

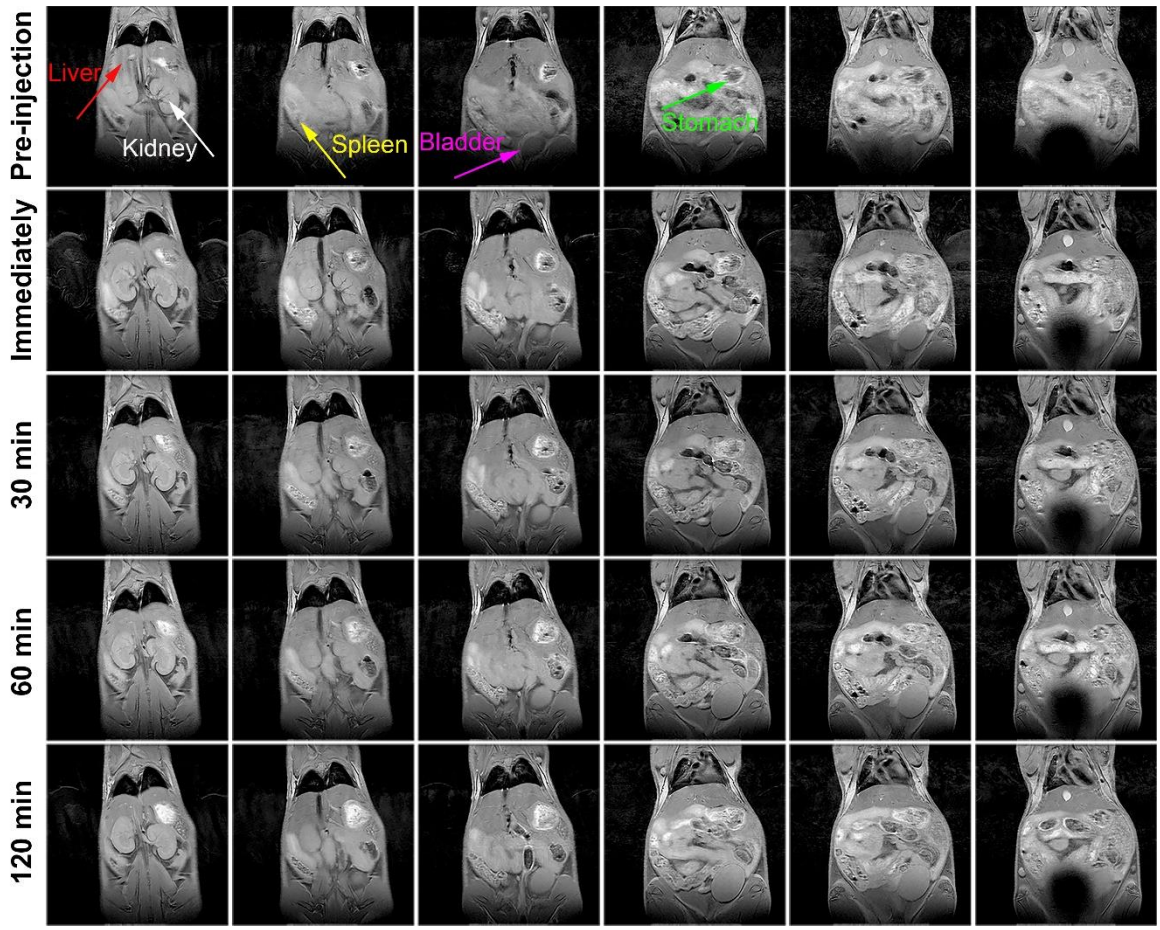

Figure S11. The coronal planes of T_1-weighted MR images of mice pre-injection, immediately after injection and 30, 60 and 120 min after injection of $Ni_{0.31}Fe_{2.69}O_4$ NPs via the tail vein (1.5 mg [Fe + Ni] kg^{-1} mouse body weight). The red, white, yellow, magenta and green arrow correspond to liver, kidney, spleen, bladder and stomach, respectively.

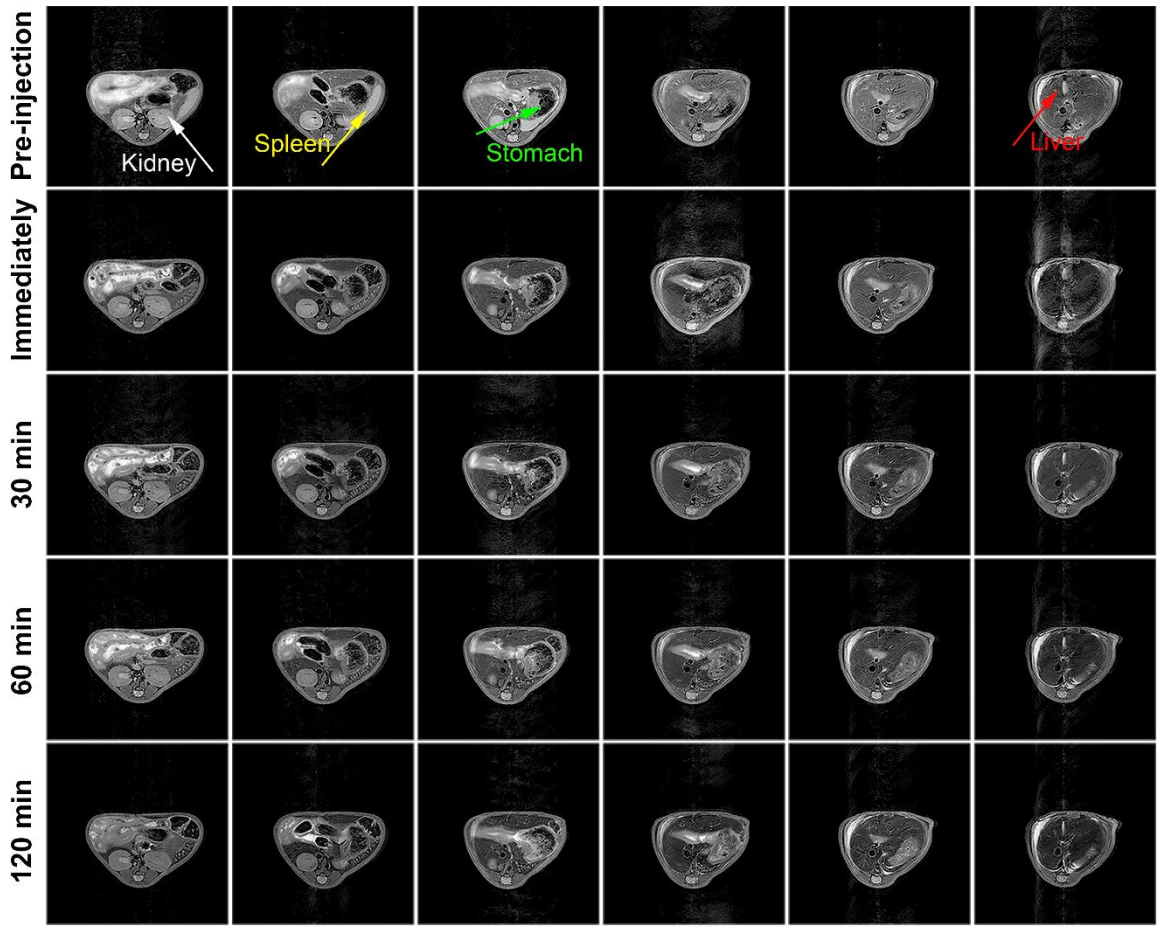

Figure S12. The transverse planes of T_2-weighted MR images of mice pre-injection, immediately after injection and 30, 60 and 120 min after injection of $Ni_{0.31}Fe_{2.69}O_4$ NPs via the tail vein (1.5 mg [Fe + Ni] kg^{-1} mouse body weight). The white, yellow, green and red arrow correspond to kidney, spleen, stomach and liver, respectively.

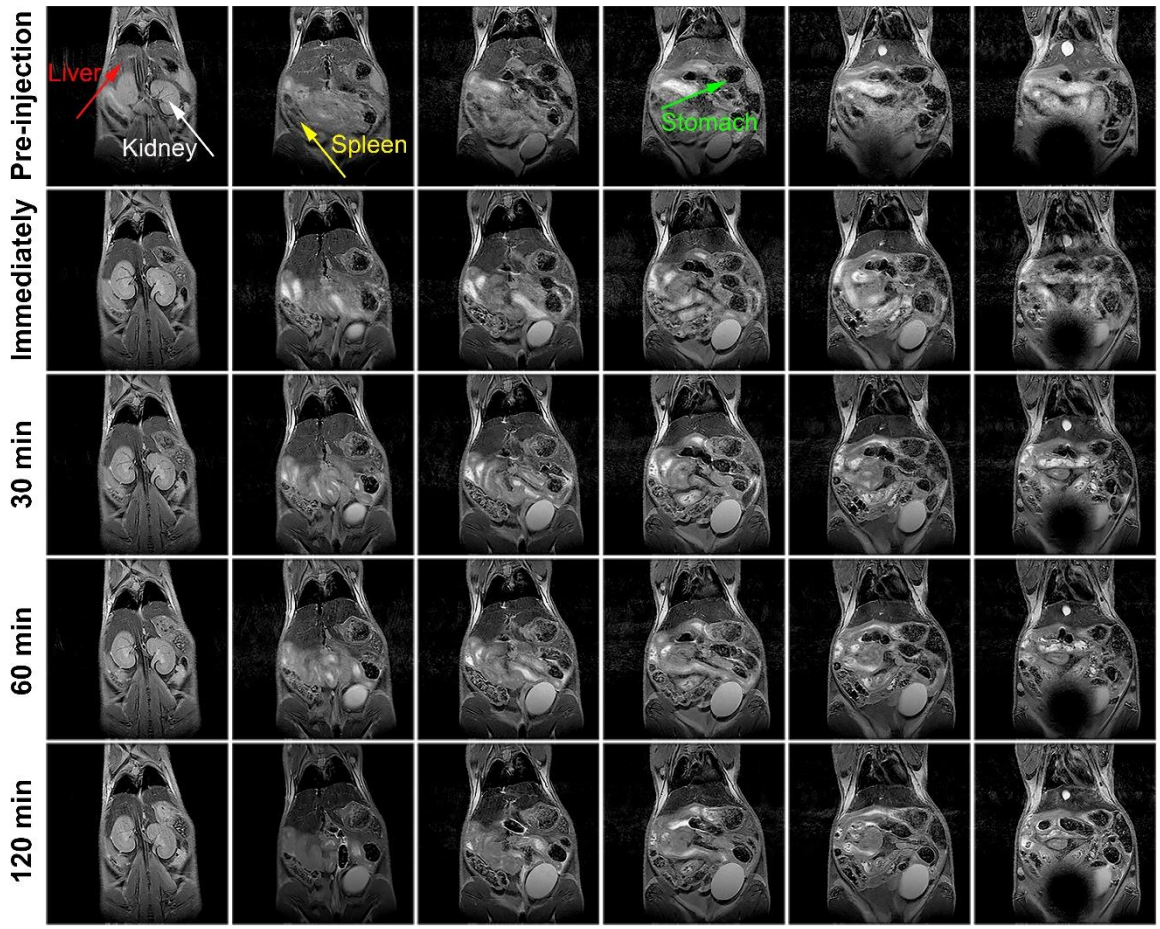

Figure S13. The coronal planes of T_2-weighted MR images of mice pre-injection, immediately after injection and 30, 60 and 120 min after injection of $Ni_{0.31}Fe_{2.69}O_4$ NPs via the tail vein (1.5 mg [Fe + Ni] kg^{-1} mouse body weight). The red, white, yellow and green arrow correspond to liver, kidney, spleen and stomach, respectively.

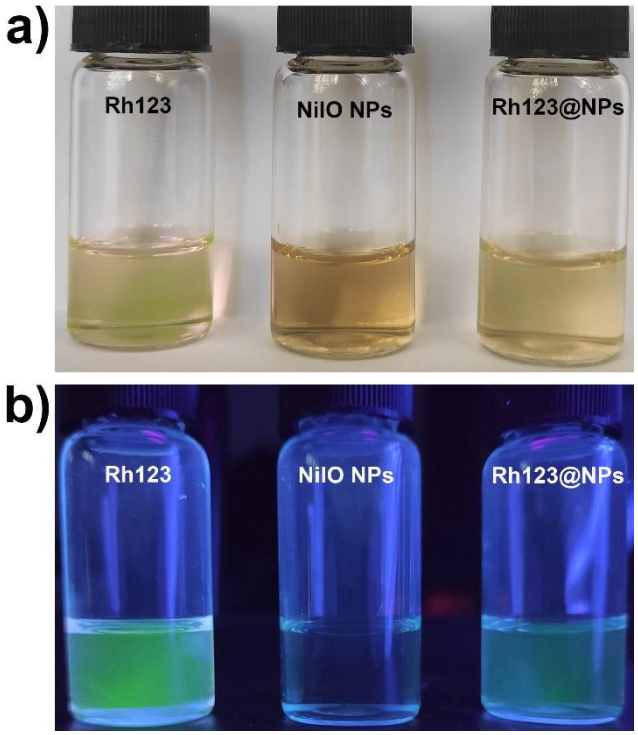

Figure S14. Photographs of Rh123, PEG@$Ni_{0.31}Fe_{2.69}O_4$ NPs and Rh123@ $Ni_{0.31}Fe_{2.69}O_4$ NPs under light (a) and in dark (b) under 365 nm UV irradiation.

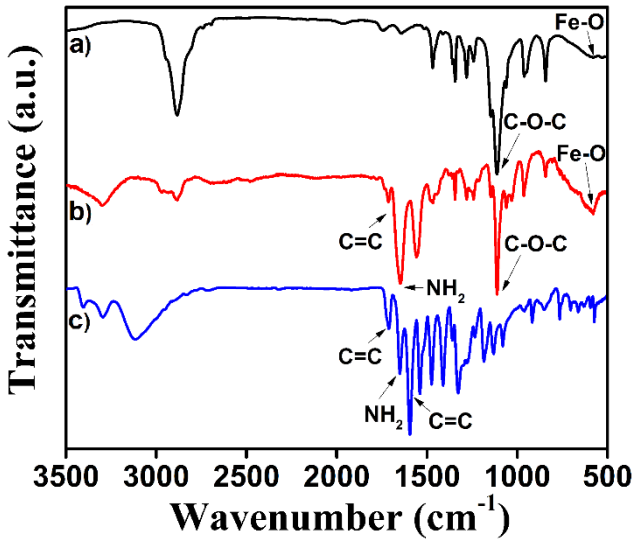

Figure S15. FT-IR spectra of (a) PEG@$Ni_{0.31}Fe_{2.69}O_4$ NPs, (b) Rh123@ $Ni_{0.31}Fe_{2.69}O_4$ NPs and (c) Rh123. Compared with PEG-modified NiIO NPs, Rh123-conjugated NiIO NPs exhibits stretching vibrations of C=C around 1652 cm^{-1} and bending vibrations of NH_2 around 1630 cm^{-1}, indicating that Rh123 was successfully grafted onto the surface of the nanoparticles.

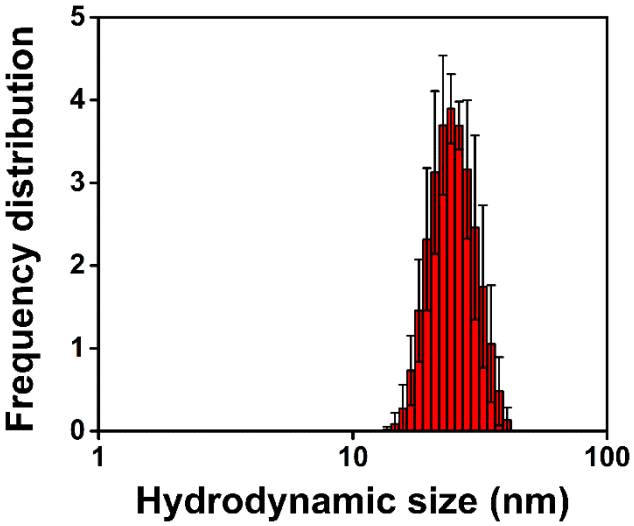

Figure S16. The hydrodynamic size distribution of Rh123@$Ni_{0.31}Fe_{2.69}O_4$ NPs in aqueous solution. The hydrodynamic size of Rh123-conjugated $Ni_{0.31}Fe_{2.69}O_4$ NPs in aqueous solution is 25.50 ± 1.71 nm, which is slightly larger than that of the particles before conjugation.